Eur. J. Mineral., 36, 433–448, 2024
https://doi.org/10.5194/ejm-36-433-2024

European Journal of Mineralogy
Open Access

First in situ Lu–Hf garnet date for a lithium–caesium–tantalum (LCT) pegmatite from the Kietyönmäki Li deposit, Somero–Tammela pegmatite region, SW Finland

Krisztián Szentpéteri[1], Kathryn Cutts[1], Stijn Glorie[2], Hugh O'Brien[3], Sari Lukkari[3], Radoslaw M. Michallik[3], and Alan Butcher[3]

[1]GTK – Mineral Potential Research Group (MTR), Espoo 02151, Finland
[2]Department of Earth Sciences, University of Adelaide, Adelaide, SA 5005, Australia
[3]GTK – Circular Economy Group (KTR), Research Laboratory, Espoo 02151, Finland

Correspondence: Kathryn Cutts (kathryn.cutts@gtk.fi)

Received: 3 September 2023 – Revised: 8 January 2024 – Accepted: 22 March 2024 – Published: 3 June 2024

Abstract. The in situ Lu–Hf geochronology of garnet, apatite, fluorite, and carbonate minerals is a fast-developing novel analytical method. It provides an alternative technique for age dating of accessory minerals in lithium–caesium–tantalum (LCT) rare-element (RE) pegmatites where zircon is often metamict due to alteration or radiation damage. Currently most dates from Finnish LCT pegmatites are based on columbite-group minerals (CGMs), but their occurrence is restricted to mineralised zones within the pegmatites. Accessory minerals such as garnet and apatite are widespread in both mineralised and unmineralised LCT pegmatites. Lu–Hf dating of garnet and apatite provides an exceptional opportunity to better understand the geological history of these highly sought-after sources for battery and rare elements (Li, Nb, Ta, Be) that are critical for the green transition and its technology. In this paper we present the first successful in situ Lu–Hf garnet date of 1801 ± 53 Ma for an LCT pegmatite from the Kietyönmäki deposit in the Somero–Tammela pegmatite region, SW Finland. This age is consistent with previous zircon dates obtained for the region, ranging from 1815 to 1740 Ma with a weighted mean $^{207}Pb / ^{206}Pb$ age of 1786 ± 7 Ma.

1 Introduction

Understanding the timing of pegmatite formation and emplacement is critical for deciphering how pegmatites have formed and thus identifying suitable regions for future exploration. The current global shift towards green energy sources makes the discovery and understanding of lithium–caesium–tantalum (LCT) rare-element (RE) pegmatites a high priority. Currently ages are determined for LCT pegmatites using U–Pb dating of columbite-group minerals or zircon (Alviola et al., 2001). However, the occurrence of columbite-group minerals is often restricted to mineralised domains, making it difficult to determine ages from unmineralised domains of pegmatites (Alviola et al., 2001). Zircon occurs commonly in LCT RE Li-pegmatites but is frequently found to be metamict (Alviola et al., 2001; Saalmann et al., 2009), resulting in poorly resolved or meaningless ages.

Recent analytical advances have made it possible to date garnet, apatite, fluorite, and carbonate minerals using an in situ Lu–Hf method (Simpson et al., 2021, 2022; Glorie et al., 2023). Garnet and apatite are both ubiquitous phases in LCT RE pegmatites within Finland; therefore, the Lu–Hf method represents a viable alternative for dating these pegmatites.

The pegmatites of the Somero–Tammela region were discovered in late 18th century and supported the local ceramic industry in Somero (Mäkinen, 1913). The Li, Cs, and rare-element enrichment of some pegmatites was recognised in the early 19th century (Aurola, 1963; Teertstra et al., 1993, 1998), and two Li-pegmatites with economic potential,

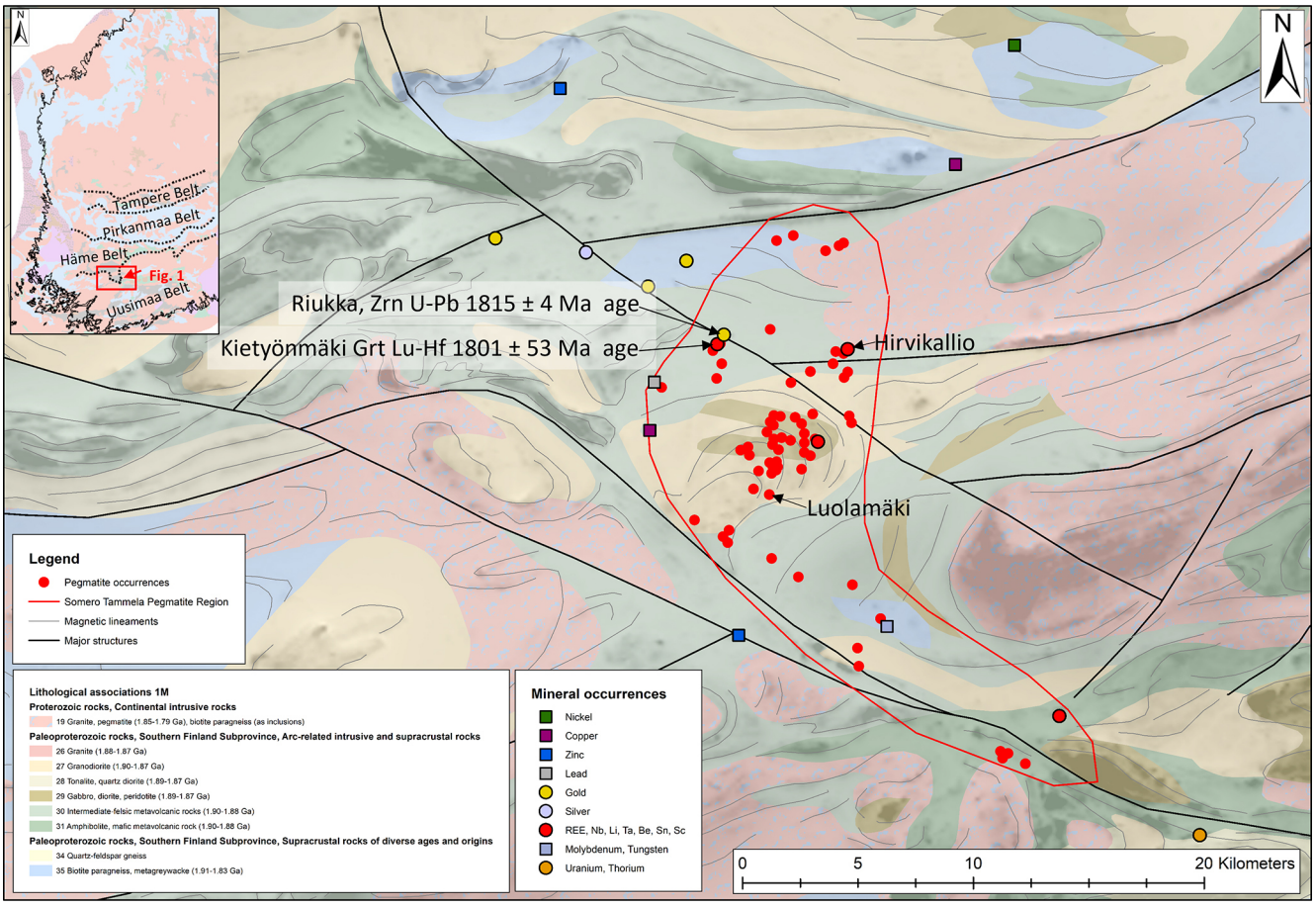

Figure 1. Regional geology map of the Somero–Tammela pegmatite region. Data source: "Bedrock of Finland" – DigiKP, digital map database, 1 : 200 000, Geological Survey of Finland, https://gtkdata.gtk.fi/mdae/index.html (last access: 21 May 2024).

Hirvikallio and Kietyönmäki, were discovered (Vesasalo, 1959; Saikkonen, 1981). The Geological Survey of Finland (GTK) investigated the Kietyönmäki occurrence in detail by surface trenching and mapping in 1983–1988 (Alviola, 1993). The results indicated that the Kietyönmäki pegmatite is considered to have the second-highest economic potential of hard-rock Li deposits in Finland (ca. 300 kt at 1.5 wt % Li_2O, non-compliant resource), after the Keliber mine district in NW Finland, which was also discovered by GTK later in 2009 (Kuusela et al., 2011). The Somero–Tammela region currently attracts many explorers. Alviola (1993) studied the deposit in detail and reported on the texture and mineralogy of the dykes, including garnet and apatite as minor mineral components. Therefore, the Kietyönmäki pegmatite offered a great test site for the first evaluation of the novel Lu–Hf dating method, based on abundant magmatic garnets and apatite easily found in some outcrops, and the existing zircon U–Pb age for the area.

In this study, we first applied the in situ Lu–Hf method to date garnet from an LCT pegmatite from the Kietyönmäki deposit in the Somero–Tammela pegmatite region, SW Finland. A detailed description of the geology and mineralogy of the pegmatite deposit is also provided to give context for the dated sample. Thus, our result represents the first successful in situ Lu–Hf pegmatite dating in Finland, opening up a great opportunity to revisit many undated pegmatite fields elsewhere in Finland and/or Fennoscandia. We have reviewed the literature and made our own field observations, sampling, sample analysis, and geology modelling based on archive drilling data to present an up-to-date review of this Li deposit with economic potential.

2 Methods

Field observations, structural measurements, and sampling were conducted during two short visits to Kietyönmäki in 2022 and 2023. Large 5–10 kg rock samples were collected to make polished slabs of > 10 cm in size. The rock samples were diamond-sawn and ground on 600-grit diamond laps at the Geological Survey of Finland (GTK) laboratory in Espoo. The slabs were analysed by a flatbed scanner, Keyence VHX-7000 digital microscope, and Hitachi SU3900 low-vacuum

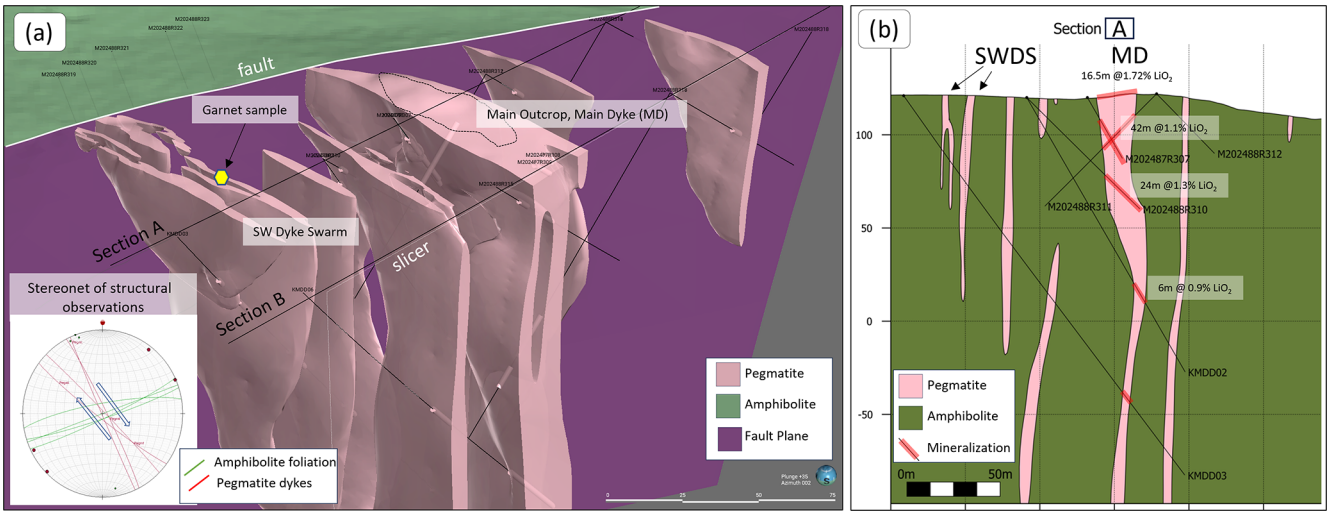

Figure 2. Simplified 3D geology model of the Kietyönmäki pegmatite deposit. **(a)** 3D model view (note compass ball for viewing angle). **(b)** Section A through the 3D geology model.

scanning electron microscope (SEM) to identify and visualise the Li minerals and their textures. Qualitative elemental analysis was carried out by the EA-300 laser-induced breakdown spectroscopy (LIBS) analytical unit on the Keyence VHX-7000 digital microscope for confirmation of RE and Li minerals and Li trace levels in minerals. Semiquantitative elemental analyses were conducted on a Hitachi SU3900 SEM equipped with an Oxford Instruments energy-dispersive X-ray spectroscopy (EDS) X-Max 20 nm^2 (SDD) using AZtec software. Minerals were identified from backscattered electron (BSE) imaging, and elemental maps were scanned over the sample area. The instrument used requires no sample preparation and offers the ability to map and image large samples such as rock slabs up to 5 kg and 20 cm in diameter. Minerals were manually analysed by collecting EDS spectra for 10 s from each mineral grain. The software converts the EDS spectra into chemical compositions. The results are normalised to 100 %. The run conditions were 20 kV accelerating voltage and 1 nA probe current. Electron microprobe analyser (EMPA) analysis on garnets used for Lu–Hf dating was performed with a (JEOL JXA-iHP200F) field-emission electron microprobe analyser (FE-EMPA) at the GTK using the WDS (wavelength-dispersive spectrometry) technique. The accelerating voltage and beam current were 15 kV and 20 nA, respectively. A defocused beam diameter set to 10 µm was used for the apatite and a 1 µm beam was used for the Ti-oxides. Analytical results have been corrected using the XPP online correction programme (Pouchou and Pichoir, 1991). Natural and synthetic minerals and metals were used as standards. Additionally, a geological 3D model was created by Leapfrog Geo software by Seequent. The "pegmatite"–lithology intercepts and the surface map (Alviola, 1993) were used for simplified modelling.

One garnet-bearing sample was prepared in a 25 cm polished epoxy mount for in situ Lu–Hf geochronology at Adelaide Microscopy, University of Adelaide, Australia. The garnet Lu/Hf ratio analyses were conducted in a single analytical session using a RESOlution-LR 193 nm excimer laser ablation system, coupled to an Agilent 8900 inductively coupled plasma–tandem mass spectrometry (ICP-MS/MS) instrument. The laser beam diameter was set to 173 or 120 µm, depending on the grain size, and ablation was conducted at a 10 Hz repetition rate and a fluence of $\sim 3.5\,J\,cm^{-2}$. The laser-based Lu–Hf method uses an NH_3–He gas mixture in the reaction cell of the mass spectrometer to promote high-order reaction products of Hf, with a mass shift of +82, while equivalent Lu and Yb reaction products are minimal (i.e. Hf reacts at a rate of 50 %–60 %, while Lu reaction is < 0.003 %; Simpson et al., 2021). Consequently, the resulting mass-shifted (+82 amu) reaction products of $^{176+82}Hf$ and $^{178+82}Hf$ can be measured free from isobaric interferences. The ^{177}Hf was subsequently calculated from ^{178}Hf, assuming natural abundances. The ^{175}Lu was measured on mass as a proxy for ^{176}Lu (see details in Simpson et al., 2021, 2023). In addition to Lu and Hf isotopes, other trace elements, including a selection of other rare-earth elements (REEs) (details in File S1 in the Supplement), were measured simultaneously to monitor for inclusions. However, not every REE was measured as this would compromise the dwell times on the Hf isotopes required for age calculations.

Isotope ratios and trace element concentrations were calculated in LADR (Norris and Danyushevsky, 2018) using NIST610 as a primary standard (Nebel et al., 2009). Lu–Hf ages were calculated as inverse isochrons using IsoplotR (Li and Vermeesch, 2021; Vermeesch, 2018) and the ^{176}Lu decay constant of Söderlund et al. (2004; $0.0001867 \pm 0.00000008\,Ma^{-1}$). The isochron was an-

Figure 3. The main spodumene-bearing pegmatite dyke (MD) looking towards NE is well exposed on a large outcrop on the top of Kietiönahde Hill. The location of the GTK's channel sampling and the channel sampling site are shown in the inset.

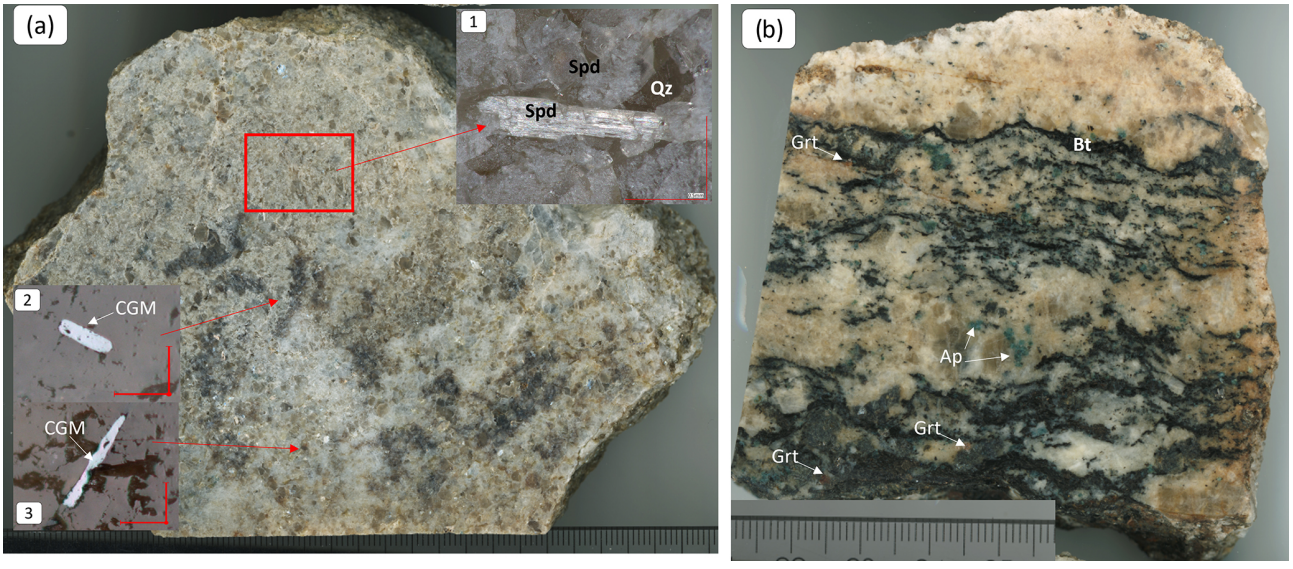

Figure 4. **(a)** Example of massive and fine-grained spodumene mineralisation of the main dyke. White spodumene (inset 1) occurs in 1–3 mm subhedral-to-euhedral prismatic crystals intergrown with quartz, albite, K-feldspar, and muscovite. Microscopic platelets of columbite–tantalite-group minerals (CGMs) are disseminated through the groundmass as 100–400 µm sized laths (inset 2, 3). **(b)** Banded albite pegmatite of the SE dyke swarm consists of distinct undulating thin layers of biotite–apatite–garnet, with quartz–albite–green apatite.

chored to an initial $^{177}Hf/^{176}Hf$ composition of 3.55 ± 0.05, which spans the entire range of the terrestrial reservoir (cf. Simpson et al., 2022). Garnet from the Högsbo pegmatite was used as a secondary reference material to correct the Lu/Hf ratios for matrix-dependent elemental fractionation. The correction factor is based on the difference between the measured and reference pegmatite crystallisation age, which is a columbite U–Pb date of 1029 ± 1.7 Ma (Romer and Smeds, 1996; Simpson et al., 2021). The uncertainty in the Högsbo garnet age is subsequently propagated to the isochron age uncertainty in the analysed samples (Table S1 in the Supplement). NIST610 glass was also used to estimate trace element concentrations in garnet using Al as the inter-

nal standard element. More details on the analytical approach can be found in Simpson et al. (2021, 2022).

Trace element mapping of a garnet grain was performed by laser ablation–inductively coupled plasma–mass spectroscopy (LA-ICP-MS) at the GTK, using a Nu AttoM single-collector (SC)-ICP-MS (Nu Instruments Ltd., Wrexham, UK) and an Analyte Excite 193 nm ArF laser ablation system (Teledyne Photon Machines, San Diego, CA, USA). The analysis was performed by the Chromium v.2 software with mapping mode using line sampling in continuous-scan mode. The lines were 1000 µm long with 10 µm spacing covering an approximate 1 mm by 1 mm area by 101 lines in total. The spot spacing on the line was 10 µm. The laser was run at 10 µm s^{-1} speed at a pulse frequency of 20 Hz and a pulse energy of 5 mJ at 35 % attenuation to produce an energy flux of 1.09 J cm^{-2} on the sample surface with a 10 µm square spot size. Analyses were made using time-resolved analysis (TRA) with continuous acquisition of data for each line. Each line analysis was initiated with a 20 µm s^{-1} preablate line scan and 15 s washout time. Then 15 s baseline measurement was followed by 104.3 ± 0.1 s signal acquisition on each line with a 5 s pause to allow the signal to come down to the baseline after each line. The total run time was 7 h including bracketing of samples by standards approximately every 1–1.5 h. Primary standards NIST610 and NIST612 were used including external standards of BHVO and BCR. Data reduction and image processing were performed using Iolite 4 software (Paton et al., 2011), loading the TRA data files for each line and the laser log file saved by Chromium v.2. Images were processed both in the "input channel", i.e. intensity maps, and using standards and baseline reduction for quantified maps according to cell-space imaging procedures of Paul et al. (2012). The following isotopes were measured during line scanning: ^{6}Li, ^{7}Li, ^{9}Be, ^{11}B, ^{23}Na, ^{24}Mg, ^{27}Al, ^{29}Si, ^{43}Ca, ^{44}Ca, ^{45}Sc, ^{47}Ti, ^{49}Ti, ^{51}V, ^{52}Cr, ^{53}Cr, ^{55}Mn, ^{57}Fe, ^{59}Co, ^{63}Cu, ^{66}Zn, ^{69}Ga, ^{72}Ge, ^{75}As, ^{77}Se, ^{85}Rb, ^{88}Sr, ^{89}Y, ^{91}Zr, ^{93}Nb, ^{95}Mo, ^{111}Cd, ^{115}In, ^{120}Sn, ^{121}Sb, ^{124}Te, ^{133}Cs, ^{137}Ba, ^{139}La, ^{140}Ce, ^{141}Pr, ^{146}Nd, ^{147}Sm, ^{153}Eu, ^{157}Gd, ^{159}Tb, ^{163}Dy, ^{165}Ho, ^{166}Er, ^{169}Tm, ^{172}Yb, ^{175}Lu, ^{178}Hf, ^{181}Ta, ^{182}W, ^{205}Tl, ^{208}Pb, ^{209}Bi, ^{232}Th, and ^{238}U. Image interrogation tools (Petrus et al., 2017) were used to create regions of interest (RoIs) and line profiles as well as chondrite-normalised REE plots from the quantified images.

3 Geology of the Somero–Tammela pegmatite province

The Somero–Tammela pegmatite region (Fig. 1) is located within the Svecofennian crustal and SW Finland tectonic provinces, in the ENE–WSW-trending Häme volcanic belt. The Häme Belt comprises volcanic rocks with minor greywackes and metapelitic units and is intruded by syntectonic plutonic rocks and late-tectonic K-granites and pegmatite dykes (Eilu et al., 2012). The Häme Belt is highly prospected, throughout, for base metal and gold resources (Saalmann, 2007; Eilu et al., 2012), but RE pegmatites containing LCT/Li types only occur in the Somero–Tammela township region within a ca. 300 km^2 area, catalogued as the "Li F005" metallogenic province by the GTK (Eilu et al., 2012). The Somero–Tammela region contains 56 known RE pegmatites (Fig. 1), with 9 containing lithium minerals. According to Alviola (2003), the lithium pegmatites belong to the LCT (Li, Cs, Ta) family of Černý (1991). The two most significant lithium pegmatite deposits are Hirvikallio and Kietyönmäki. The Hirvikallio petalite pegmatite is 170 m long and 5–25 m wide. It contains 200 kt at 1.78 wt % Li_2O to a depth of 50 m. The Kietyönmäki dyke swarm is composed of several Li-bearing pegmatites, of which the largest is 200 m long and 10 m wide (Alviola, 1989). It contains 300 kt at 1.5 wt % Li_2O. However, according to mineral prospectivity modelling (MPM) studies by Leväniemi (2013), the province has a large area of high pegmatite potential.

Based on our GIS compilation (Fig. 1), the Somero–Tammela pegmatite region is located within an apparent intersection of older ENE–WSW-trending and younger NW–SE-trending regional structural zones. The early Svecofennian syn-tectonic structures, folds, foliation, and major shear zones are responsible for the N–S stacking of ENE–WSW-trending belts of plutonic microcline granite (Eilu, 2015) to the south and granodiorite–gabbro composite intrusions mantled by volcanic rocks and metasediments in the central-north of the Somero–Tammela pegmatite region (Fig. 1). The largest concentration of LCT pegmatites occurs within the granodiorite–gabbro intrusive complex centred on mappable bodies of granite pegmatite, north of the Luolamäki Cs, Be, (Li) pegmatite deposit (Fig. 1). However, significant Li concentrations are only found distally, 5–7 km to the north-northwest within metavolcanics and metasediments in the two deposits with economic potential, Kietyönmäki and Hirvikallio (Figs. 1, 2).

The only radiometrically age-dated pegmatite within the region is the Kietyönmäki (or Riukka) pegmatite, although this was part of a study investigating gold mineralised quartz veins and pegmatites (Saalmann et al., 2009). U–Pb dating of zircon from a pegmatitic quartz–feldspar dyke produced a weighted mean ^{207}Pb / ^{206}Pb age of 1786 ± 7 Ma. (https://gtkdata.gtk.fi/mdae/index.html, last access: 23 May 2024; and Saalmann et al., 2009). The investigated zircons contained older-age domains up to a maximum ^{207}Pb / ^{206}Pb age of 1815 ± 4 Ma and were very U-rich (Th / U ∼ 0.00–0.03), making them extremely sensitive to radiogenic lead loss. As such, Saalmann et al. (2009) interpreted that the older age of ca. 1815 Ma more likely represents the emplacement age of the pegmatite. There are very few age dates available from W and S Finland LCT pegmatites, and they are based on columbite U–Pb geochronology indicating 1803 ± 3 Ma (Lindroos et al., 1996) for the Kemiö pegmatite province in the Uusimaa Belt. The pegmatites of the Seinäjoki area in

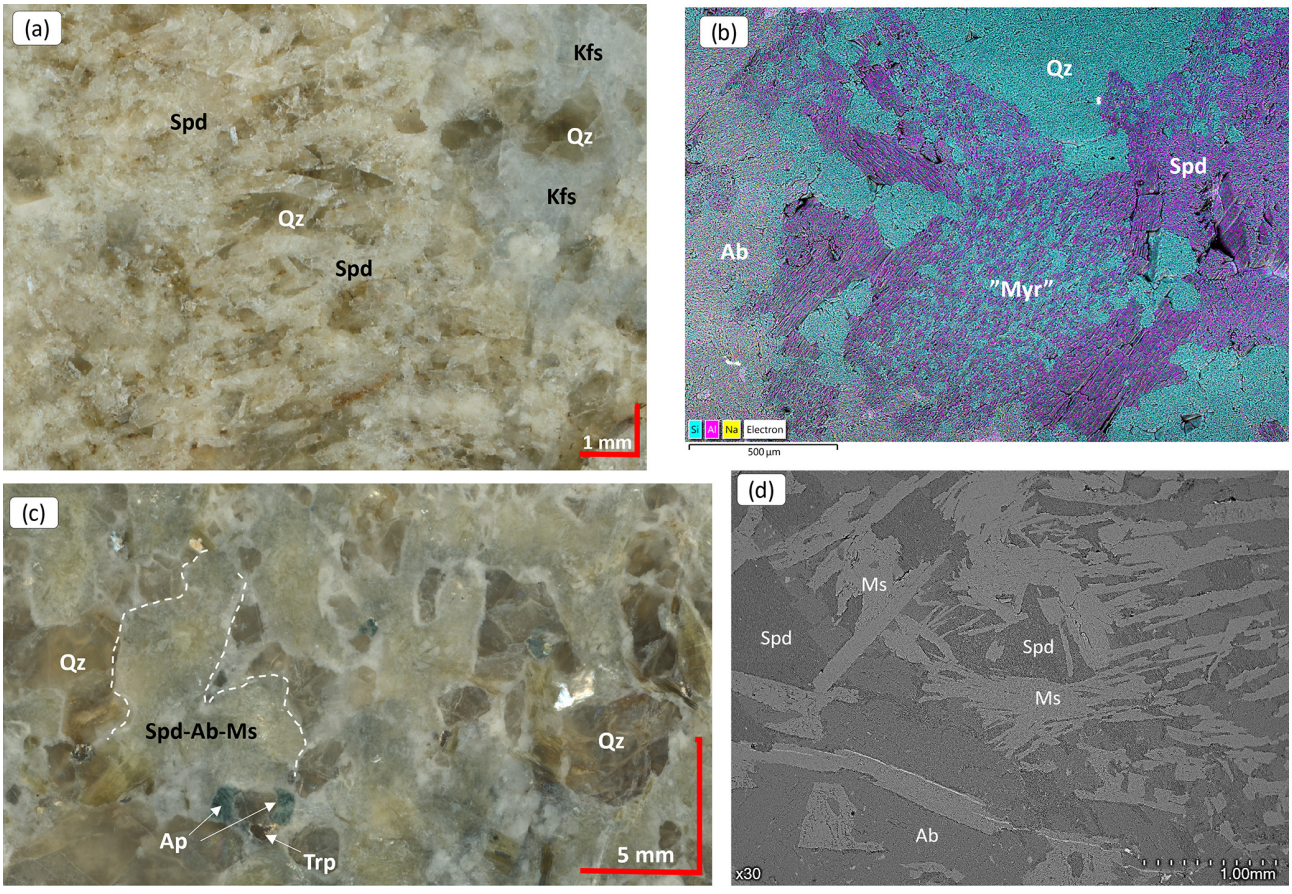

Figure 5. **(a)** Digital microscope view of the spodumene pegmatite of the main dyke (MD). Platy elongated white spodumene (Spd) can be easily seen intergrown with quartz (Qz) (the texture most reminiscent of common SQI symplectite after petalite) and K-feldspar (Kfs), but the anhedral white masses cannot be resolved very well. **(b)** SEM–BSE elemental mapping, using Si–Al–Na as the RGB colour composite on top of the BSE electron image reveals that those white anhedral masses on the optical images consist of fine myrmekitic intergrowths ("Myr") of spodumene (Spd) and quartz (Qz) along with subhedral platy spodumene and albite (Ab). **(c)** Digital microscope view, which shows blocky yellow-white clouded pseudomorphs of spodumene–albite–muscovite (Spd–Ab–Ms) aggregates potentially as an alteration product of earlier petalite and brown "FeMnLi-phosphate" (Trp) with green apatite (Ap). **(d)** SEM–BSE image shows the composition and texture of these pseudomorphs.

Ostrobothnia were more extensively age-dated, and Alviola et al. (2001) concluded that the pegmatites fall into two age groups: the niobium–yttrium–fluorine (NYF) family of pegmatites, such as the Alavus REE pegmatites, crystallised at 1.86 Ga, and other pegmatites, i.e. the pegmatites of the LCT family, formed much later at 1.80–1.79 Ga in the Seinäjoki and Kaustinen provinces.

The existing age data and excellent pegmatite outcrops with visible garnets at the Kietyönmäki location have provided the opportunity for trialling the novel Lu–Hf garnet geochronology method (Simpson et al., 2021). This is the first time this method has been applied in Finland to garnet in a Li-pegmatite.

4 Research and exploration history of the Kietyönmäki pegmatite

The area was first prospected by Swedish geologists, who discovered Cu-sulfide mineralisation, which attracted more explorers to the area (Aurola, 1963). Soon pegmatite occurrences were discovered, and quartz was found to be suitable for glass manufacturing, processed in smelting plants built in the town of Somero. Pegmatite mining exposed a lot of material, and subsequently, rare minerals and metals became known through investigations by Nils Nordemskiöld (see Mäkinen, 1913). The first geology map sheet of the area was published in the early 1900s by Jakob Johannes Sederholm (Aurola, 1963), and then updated maps, already showing locations of pegmatites, with descriptions were published by Mäkinen (1913) and later by Simonen (1956). The first detailed study and classification of pegmatite types were un-

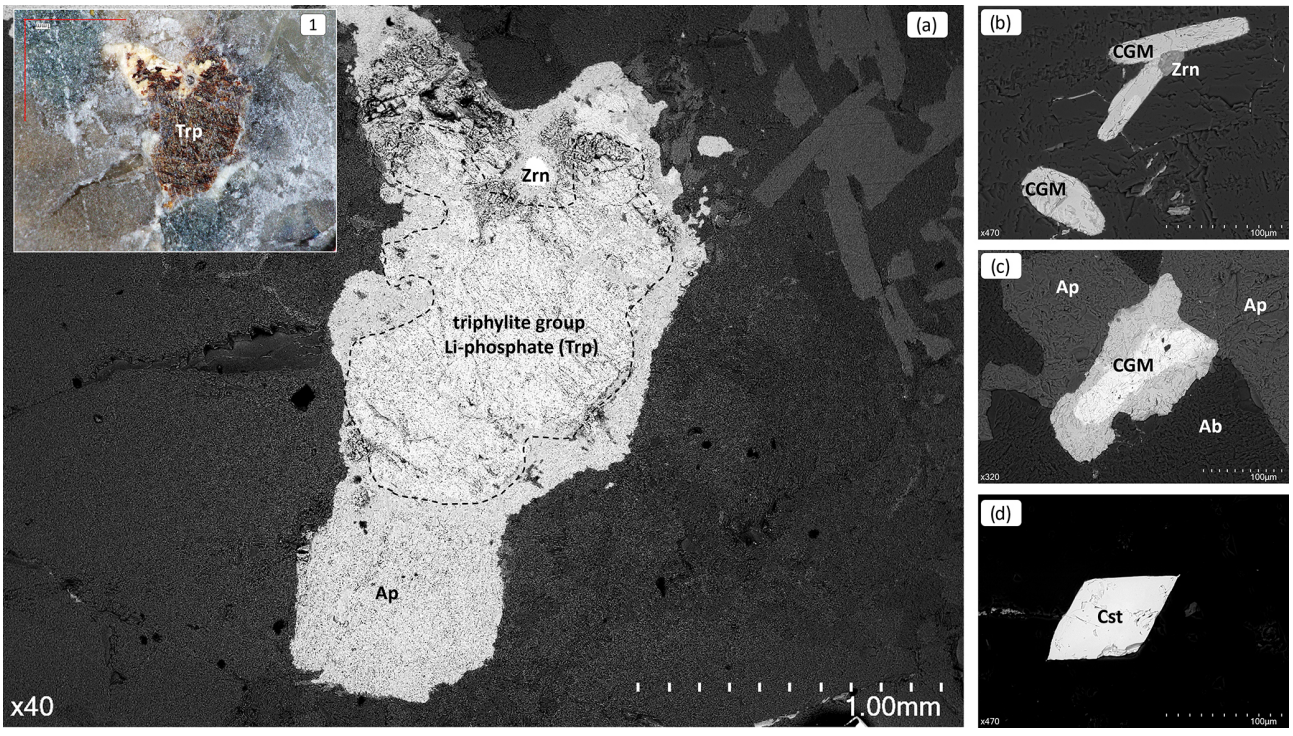

Figure 6. SEM–BSE images of Li-phosphate and RE minerals. **(a)** Secondary "FeMnLi-phosphate" triphylite-group (Trp) intermediate phase surrounded by apatite (Ap). Inset 1 shows the optical image with a distinct brown colour. **(b)** CGM platelets (CGM) and zircon (Zrn) in albite. Note the brighter core with a higher Ta concentration. **(c)** A zoned CGM grain with a distinct brighter core of higher Ta concentration associated with apatite (Ap). **(d)** Euhedral single crystal of cassiterite (Cst) in a quartz–albite matrix.

dertaken done by Aurola (1963). The RE-rich pegmatite minerals attracted trace element studies in K-feldspar and pollucite from the Loulamäki pegmatite (Teertstra et al., 1993, 1998) and the unique massive petalite deposit of Hirvikallio (Vesasalo, 1959; Saikkonen, 1981).

The Kietyönmäki Li-pegmatite occurrence was first investigated, utilising modern and systematic exploration, by the GTK in 1983–1988 with surface sampling, ground magnetics, and diamond drilling (Alviola, 1993). A total of 17 diamond holes were drilled on three traverses for a total of 884.45 m. Mineralised pegmatite dykes were confirmed to a depth of about 50 m b.s. (below surface) with intercepts (in hole R310) of 24 m at 1.31 % Li_2O, including 3 m at 3.6 % Li_2O. Exploration potential remained open to the south along strike and downdip. To the north, the pegmatite swarm is offset by an ENE-trending fault (Fig. 2).

In 2016 Sunstone Metals (formerly Avalon Minerals) joint venture with Scandian Metal Pty Ltd. completed six diamond drill holes totalling 1171.9 m, confirming the high-grade spodumene-bearing pegmatite dyke swarm, with hole KMDD001 returning 24.2 m at 1.4 % Li_2O. In 2021 the prospect was acquired by United Lithium Corp., a Canadian company, and they announced additional further drilling that started in late 2022. A first-stage 10-hole drill programme was planned, with holes averaging 100 m in length aiming to confirm a mineralised body exceeding 0.5 Mt at > 1 wt % Li_2O. Results have been reported for a total of 1450 m of diamond drilling in 13 holes as of late 2023, confirming 205 m of drilled strike length and a depth extension of 160 m below the surface for the main dyke.

5 Geology and petrography of the Kietyönmäki pegmatite

5.1 Review of 3D geology

The GTK's drilling database was used for simple geological 3D modelling to understand and summarise the geometry and extent of the dyke swarm. The four additional holes drilled by Sunstone Metals (KMD001, KMD002, KMD003, KMD006) were digitised (for pegmatite intersections) from sections published on company websites. A simplified 3D geology model was built by Leapfrog Geo (Fig. 2a). The modelling indicates that the pegmatite swarm contains at least six NW-trending dykes within a 200 m wide corridor with a strike length of at least 150 m NW–SE and with vertical to 70° SW dips. The main dyke (MD) is the most continuous along strike and depth and is the most consistently Li-mineralised (Fig. 2b). It was intersected 100–130 m b.s. at both section A and section B with still significant 17 m true thickness on section B with a total of 11 m Li mineralisa-

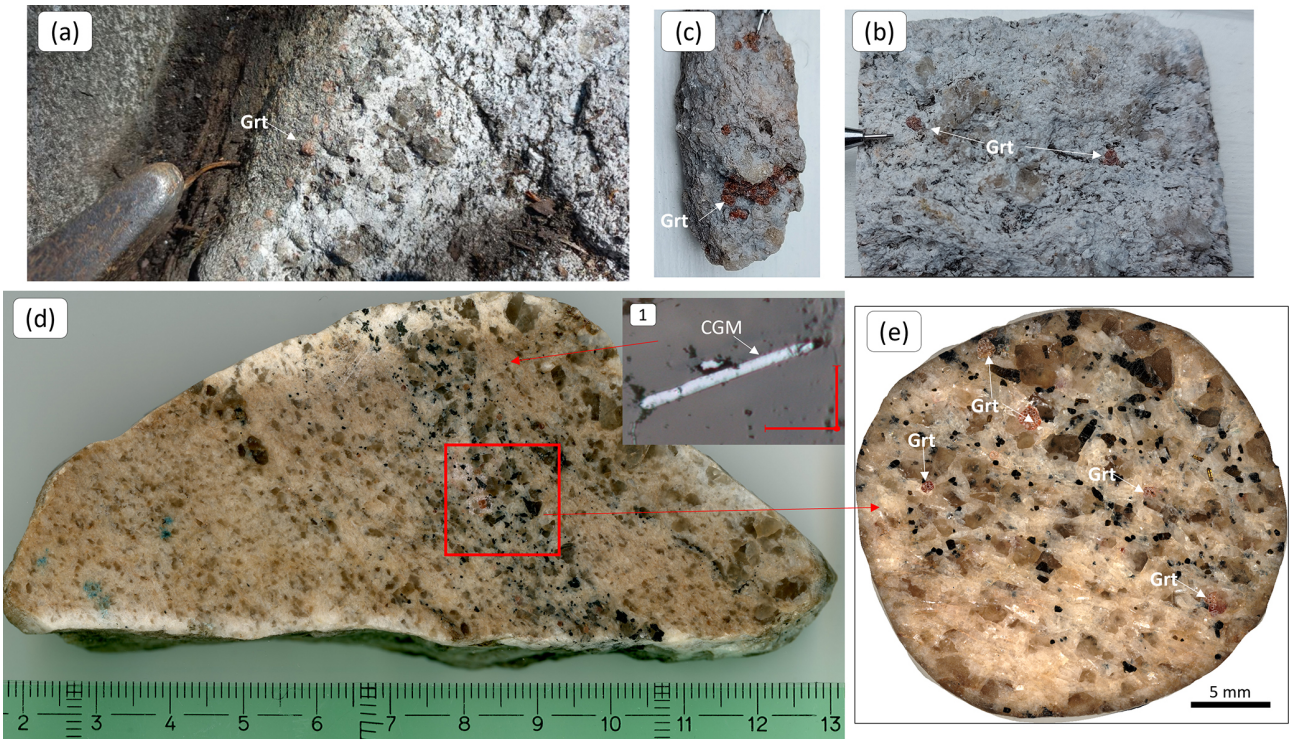

Figure 7. Examples of garnet occurrences in the SE swarm albite pegmatite dykes. **(a)** Garnet grains aligned along the contact margin of the dyke. **(b, c)** Single garnet grains in a quartz–feldspar matrix. **(d)** Tourmaline and garnet grains in an albite–quartz matrix and garnet–tourmaline bands in an albite–quartz matrix with green-blue apatite, with CGM minerals in the matrix (inset 1). **(e)** Surface scan of a polished epoxy mount dated using the Lu–Hf method.

tion, including 2 m at 1.9 % Li_2O and 9 m at 0.8 % Li_2O at 130 m b.s. Li-grade distribution within the MD may indicate a plunge at 144° azimuth and 70° dip, suggesting some further potential SW along strike and downdip. However, it is likely that a potential open-pit resource is contained within the outcropping MD and down to about 100 m b.s., which United Lithium Corp. is about to define. The SW dyke swarm is also continuous down to about 100 m but contains minor or no Li mineralisation and is restricted only to section A.

5.2 Field and petrography observations

5.2.1 Main dyke

The main dyke of the Kietyönmäki deposit is well exposed on a > 25 m long, 8–16 m wide, NNW-trending outcrop with steep vertical sides and inclusions of country rocks visible (Fig. 3). The pegmatite consists of massive and even-grained white and light-grey material. On the hand specimen scale, only quartz, muscovite, and porphyritic K-feldspar are visible in a white fine-grained (0.1–2 mm) matrix of indistinguishable Li minerals. Therefore, large rock samples were collected and slabbed and then finely ground and investigated with a digital microscope and low-vacuum SEM (Figs. 4–6) to observe the Li minerals. Smooth surfaces reveal the presence of white spodumene throughout the samples (Figs. 4a and 5a). Spodumene occurs in two textural associations: (1) well-defined subhedral-to-euhedral prismatic elongated crystals intergrown with quartz and albite (Fig. 5a). SEM–BSE imaging shows that some spodumene occurs in myrmekitic intergrowths with quartz in this association (Fig. 5b). (2) In other samples, anhedral 1–2 mm spodumene occurs as complex intergrowths with tabular muscovite and albite – forming 0.5–1 cm blocky pseudomorphs after pre-existing Li minerals spodumene or petalite (Fig. 5c, d). These textural features, the mineral assemblage, and the fine grain size are reminiscent of symplectite and granular SQIs (spodumene–quartz intergrowths) typical in some Li-pegmatites, suggesting a breakdown reaction from pre-existing more coarsely grained petalite (Černý and Ferguson, 1972; Thomas et al., 1994; London, 1984, 2008; Bradley et al., 2017; Dias et al., 2019; Lima and Dias, 2019; Roza Llera et al., 2019). However, the pseudomorphs including the muscovite (cymatolite/aglaite) could suggest many other processes such as alteration by late hydrothermal acidic fluids or reaction of K-feldspar or albite by a Li fluid as well as breakdown due to, for example, syn-post-mineralisation pressure (Charoy et al., 2001; Martins, 2009; Chischi et al., 2021).

Both optical microscopy and SEM–BSE imaging found abundant minor (50–300 µm) inclusions of platy columbite–

tantalite-group minerals (CGMs) and subhedral–euhedral cassiterite (Figs. 4, 6, 7) The CGMs from the main dyke are homogenous and have the composition of columbite-(Fe) with Ta# (Ta / (Ta + Nb)) of 0.36 (Fig. 8). In addition, minor dark-green, blueish Mn-rich fluorapatite was found, associated with rare brown anhedral, blocky Fe, Mn-bearing Li-phosphate of the triphylite group (Fig. 5). The latter mineral was confirmed, with a combination of SEM–EDS (Fig. 6), LIBS analysis, and observation of optical properties, to be an intermediate phase in the triphylite–heterosite and lithiophilite–purpurite solid solutions, i.e. "$Li(Fe^{2+},Mn^{2+})(PO_4) \rightarrow Li_{1-x}Mn^{2+}_{1-x}\ Fe^{3+}_x(PO_4) \rightarrow (Fe^{3+},Mn^{3+})(PO_4)$" (Lyalina et al., 2023). A few pink, 1–2 mm garnet grains were observed macroscopically.

5.2.2 The SW dyke swarm

Several narrower (30 cm to 1.5 m) dykes are exposed in numerous smaller outcrops to the west of the main dyke (Fig. 9). The mafic amphibolite host rock shows clockwise deflection of the foliation along the contacts, indicating a dextral shear sense for the fault zone in which the pegmatites were emplaced (Fig. 9). The dykes often show weak to moderate magmatic foliation parallel to the walls, marked by darker bands rich in biotite, garnets, and blue apatite (Figs. 4b, 7). Garnets of 0.5–3 mm in size can be observed throughout the dykes from rim to core, often associated with black tourmaline (schorl) and/or biotite (Fig. 7). Garnet is most abundant in the outcrops of the SW dyke swarm. Orange, pinkish garnet occurs in 1–3 cm flow bands associated with tourmaline and/or biotite and blue-green apatite (Figs. 4, 7, and 10). The grain size is generally fine (0.1–3 mm) but can be somewhat variable (smaller than 4–5 mm). Due to its higher abundance, the garnet targeted for Lu–Hf geochronology was sampled from one of the dykes from the SW dyke swarm.

Small pockets of coarse quartz ± schorl occur in some dykes. Digital and SEM microscopy studies of the cut and ground rock slabs reveal that most of these dykes are composed of quartz–albite–muscovite–biotite–tourmaline–garnet–apatite (Figs. 7, 10). Li minerals were not observed in the studied sample, but CGMs were found at the same abundance as in the main dyke. Most CGMs occur as minor 50–200 µm platelets with homogenous columbite-(Fe) composition, but a few grains had brighter (Fig. 6) cores on the BSE images corresponding to a Ta-rich (up to tantalite-(Fe)) core and Nb-rich rims in these simply zoned grains (Fig. 8, Table 1). The CGMs in the SW dyke swarm are less evolved (Ta# 0.15–19) compared to the CGMs in the MD (Ta# 0.37) (Fig. 8). However, one core of a CGM in the SW dyke swarm has the highest Ta# 0.52, corresponding to a tantalite-(Fe) composition. Compositional zoning observed in these grains is reverse zoning. Based on homogenous and simple- and reverse-zoned textures, the CGMs all appear to be primary magmatic minerals at Kietyönmäki (Černý, 1989; Černý et al., 1992a; Černý et al., 1986; Tindle and Breaks, 2000), despite the apparent multistage formation/alteration of the Li minerals in the MD. Compositional variation trends in CGMs (Fig. 8) are not obvious based on the limited number of observations but may fall in the spodumene or spodumene–petalite pegmatite trends with low Ta and slightly increasing Mn (Anderson et al., 2013; Pan and Breaks, 1997; Breaks and Tindle, 1997). The reverse zoning and differing Ta# numbers between the MD and SW dyke swarm may indicate emplacement of the Kietyönmäki pegmatite swarm in multiple batches with differing initial Ta / Nb in the melt (Anderson et al., 2013).

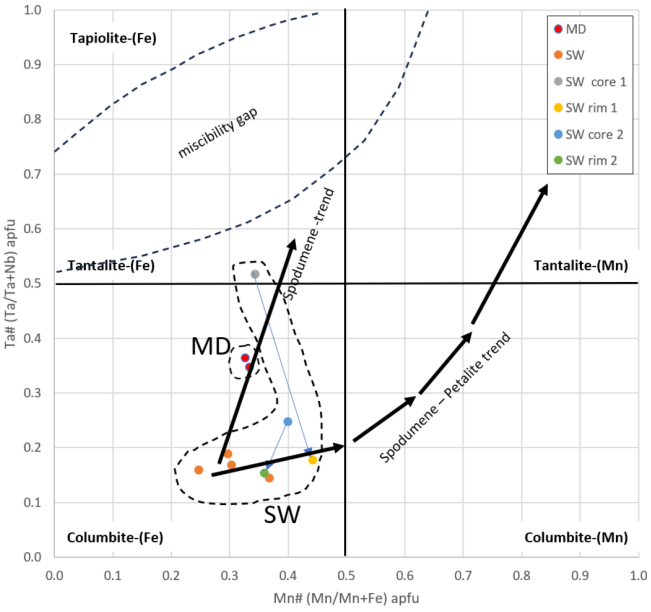

Figure 8. SEM–EDS compositions of CGM (MD – main dyke; SW – southwest dyke swarm) core and rim analyses plotted on the CGM compositional diagram with trends after Černý (1989, 1992) and the miscibility gap by Černý et al. (1992b).

6 Lu–Hf garnet age dating

6.1 Garnet major element composition by SEM–EDS and EMPA

The major element geochemistry of garnet was studied by EMPA spot analysis and SEM–EDS elemental mapping. Elemental mapping by SEM–EDS shows that all garnets are included in albite–quartz matrix in association with tourmaline and that garnet has no major variation in Fe and Mn elemental distribution within single grains (Figs. 10, 11) at the sensitivity level of the SEM–EDS. Garnets from the sample used for Lu–Hf age dating were analysed by an EMPA, and results are reported in Table 2 and plotted in Fig. 11a. The results show an enriched (38.2–39.4 Sp) spessartine component and low Ca and Mg contents, which is typical of the

Table 1. Composition of columbite group minerals (CGMs) determined by SEM–EDS. Element oxide concentrations are in weight percent (wt %). Cation calculations are on the basis of six oxygen atoms for the stoichiometric formula XY_2O_6. Bold values are cation site occupancies from cation calculation. Ideal occupancies: PY = 2.0; PX = 1.0; PX + Y = 3.0.

	MD		SW							
				Core	Rim			Rim	Core	Rim
	27	37	102	108	109	116	117	120	121	122
Nb_2O_5	41.7	41.5	63.1	28.9	59.1	58.5	61.3	62.4	52.5	62.4
Ta_2O_5	39.9	36.8	17.8	51.6	21.3	22.8	20.8	19.7	28.8	18.9
FeO	13.7	16.3	14.0	13.0	13.7	14.5	13.7	14.4	13.4	13.8
MnO	4.4	5.4	5.1	4.4	6.0	4.2	4.1	3.5	5.3	4.9
Sum (recal.)	99.7	100	100	97.9	100	100	100	100	100	100
Nb	1.26	1.25	1.72	0.95	1.64	1.63	1.69	1.71	1.51	1.71
Ta	0.73	0.67	0.29	1.02	0.36	0.38	0.34	0.32	0.50	0.31
Σy	**1.99**	**1.92**	**2.01**	**1.97**	**1.99**	**2.01**	**2.03**	**2.04**	**2.00**	**2.02**
Fe	0.77	0.91	0.71	0.79	0.70	0.75	0.70	0.73	0.71	0.70
Mn	0.250	0.303	0.259	0.272	0.310	0.221	0.212	0.180	0.284	0.251
Σx	**1.02**	**1.21**	**0.96**	**1.06**	**1.01**	**0.97**	**0.91**	**0.91**	**0.99**	**0.95**
$\Sigma x + y$	**3.01**	**3.13**	**2.98**	**3.04**	**3.01**	**2.98**	**2.95**	**2.95**	**3.00**	**2.97**
Ta#	0.365	0.348	0.145	0.518	0.178	0.190	0.169	0.159	0.248	0.154
Mn#	0.325	0.333	0.367	0.343	0.441	0.296	0.303	0.247	0.400	0.359

Ta# = Ta/(Ta + Nb), and Mn# = Mn/(Mn + Fe).

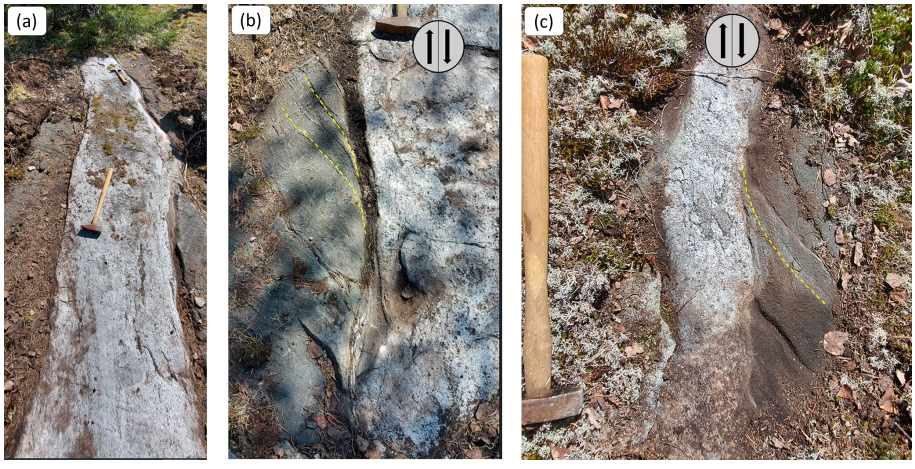

Figure 9. **(a)** Example of a smaller dyke in the SE dyke swarm albite pegmatite. Weak-to-moderate magmatic flow banding can be observed. **(b)** Deflection of the near-vertical foliation plane (shown by dashed yellow lines) in the metavolcanic bedrock along a 1 m wide dyke contact. **(c)** Deflection of the foliation along a 20 cm wide dyke contact. The clockwise rotation of the foliation plane suggests a dextral shear sense of the ENE-trending shears zones along which the Kietyönmäki pegmatite dykes were emplaced.

LCT pegmatite garnet compositional field and of a weakly to moderately evolved pegmatite (Müller et al., 2012; Moretz et al., 2013; Hernández-Filiberto et al., 2021) (Table 2). This moderately evolved composition may explain the lack of Li minerals in the garnet-bearing albite pegmatites of the SW swarm. LIBS analysis and mapping indicate the presence of Li in the garnet structure (Fig. 11b). The observed Li (671 nm) signal intensity of ca. 500–550 counts corresponds to a maximum 161 ppm Li quantified by LA-ICP-MS mapping (see Sect. 6.2).

6.2 Garnet trace element mapping by LA-ICP-MS

One solitary, euhedral grain of orange-coloured garnet was selected for LA-ICP-MS line mapping (Fig. 12). A rectangular area of 1000 × 1000 µm was used to fully cover a target grain. Time-resolved analysis (TRA) results were processed, and elemental images were created using Iolite 4 (Paton et al., 2011; Paul et al., 2012). Relative-intensity maps were created from the background-corrected input channel signals (Fig. 12), and quantitative image maps were processed using background correction and internal standards (Fig. 12). Stan-

Table 2. Composition of garnets measured by the EMPA method.

	1	2	3	4	5	6	7	8	9	10	11	12	13	14	15	16	17
SiO_2	36.29	36.13	36.00	35.94	36.19	35.68	35.63	36.12	35.82	36.01	35.70	35.49	35.54	35.71	35.54	35.73	35.60
TiO_2	0.06	0.06	0.06	0.05	0.04	0.07	0.07	0.07	0.06	0.06	0.08	0.04	0.07	0.08	0.06	0.07	0.09
Al_2O_3	20.82	21.10	20.92	21.00	21.01	20.80	21.07	20.77	20.94	20.69	21.22	20.95	20.98	20.66	21.01	20.79	20.83
FeO	25.72	25.60	25.73	26.01	25.82	25.80	25.46	25.97	25.55	25.76	25.75	25.79	25.64	25.52	25.58	25.63	25.52
MnO	17.13	17.25	17.36	16.80	17.10	16.93	17.39	16.98	17.18	17.10	16.98	17.09	17.12	17.05	17.12	17.33	17.46
MgO	0.77	0.80	0.78	0.71	0.74	0.76	0.76	0.79	0.79	0.79	0.75	0.79	0.81	0.84	0.80	0.80	0.82
CaO	0.24	0.25	0.26	0.23	0.23	0.25	0.23	0.22	0.24	0.23	0.23	0.26	0.24	0.26	0.25	0.24	0.24
Total	101.0	101.2	101.1	100.7	101.1	100.3	100.6	100.9	100.6	100.6	100.7	100.4	100.4	100.1	100.4	100.6	100.6
Endmembers																	
Py	3.07	3.16	3.10	2.85	2.96	3.04	3.03	3.15	3.16	3.14	3.00	3.14	3.22	3.37	3.18	3.18	3.26
Alm	57.46	57.14	57.13	58.33	57.68	57.81	56.93	57.88	57.20	57.53	57.75	57.50	57.32	57.20	57.26	57.07	56.73
Gro	0.70	0.70	0.73	0.66	0.66	0.72	0.67	0.63	0.68	0.66	0.66	0.75	0.70	0.73	0.73	0.68	0.70
Sp	38.77	38.99	39.04	38.16	38.70	38.43	39.37	38.34	38.96	38.67	38.58	38.61	38.77	38.70	38.83	39.07	39.31
Sp / Alm	0.67	0.68	0.68	0.65	0.67	0.66	0.69	0.66	0.68	0.67	0.67	0.67	0.68	0.68	0.68	0.68	0.69

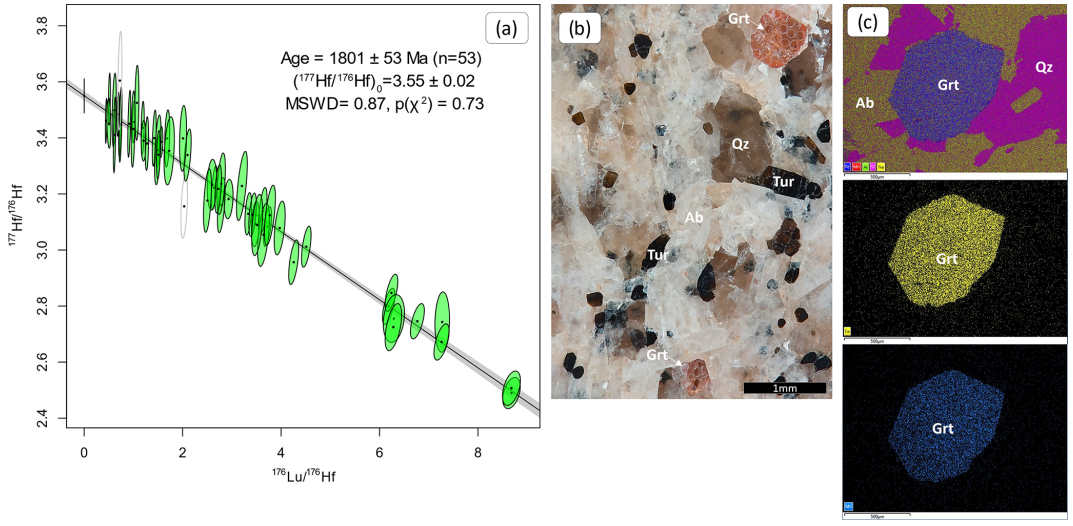

Figure 10. **(a)** Lu–Hf isochron for the Kietyönmäki sample. **(b)** Scanned image of the dated sample indicating the spot locations. **(c)** SEM–EDS maps of Kietyönmäki garnet indicating major element intensity (Fe, Mg, Al, Si, and Na) and Fe and Mg intensity.

dards used were BHVO for major elements and NIST612 for trace elements and REEs. Quality checks were made using NIST610 as an external standard and BCR. Relative-intensity maps reveal zoned distribution of trace elements: Li, V, Sc, Ga, Zn, and most of the heavy REEs (HREEs) and Y. Y zoning is most clearly defined and forms concentric face-parallel oscillatory zones with high and low concentrations gradually decreasing from core to rim with a maximum pixel value of 202 ppm and an average of 140 ppm in the core and 15 ppm in the outer rim (Figs. 12 and 13). The garnet is enriched in HREEs, especially in the core, reaching up to 150 ppm (sumHREEs) on average and decreasing towards the rim down to 10–15 ppm levels (Fig. 13). However, the total HREE concentration (sumHREEs) map strongly mimics that of Y, so Y appears to be a suitable proxy for HREEs including Lu. Quantified maps allow for the extraction of chondrite-normalised REE profiles from different growth zones, and it appears that two types of profiles are present and alternating during growth. Domain 1 (D1) is characterised by the highest relative and absolute values of HREEs compared to light REEs (LREEs). In D1 the concentration of LREEs is below the limit of detection (LOD). In Domain 2 the LREEs are above the LOD, but the total concentration of HREEs is lower and the profile shows a large negative anomaly of intermediate REEs (MREEs). Li concentration is somewhat diffuse but higher (i.e. 160 ppm) in the core, roughly coeval with the area of highest trace element concentrations, and lower (118 ppm) in the rims (Fig. 12b). Sc distribution is complex (Fig. 12e) and most similar to Lu distribution (Fig. 12d). Sc has a clear low-concentration (37 ppm) rim zone with elevated concentric zones in the core (155 ppm) and areas reminiscent of sector zoning with the highest observed concentration of 185 ppm.

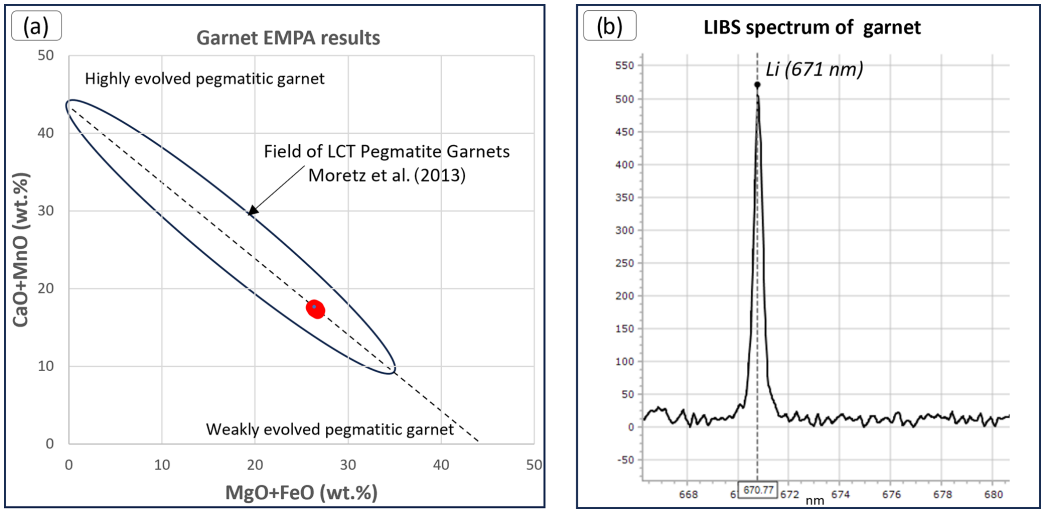

Figure 11. **(a)** Binary MgO + FeO wt % versus CaO + MnO wt % plot for garnet grains analysed by an electron microprobe analyser (EMPA) in reference to typical LCT pegmatite garnet compositions (Moretz et al., 2013) along magmatic garnet composition evolution tends. **(b)** LIBS emission spectrum of Li in garnets at 671 nm, the most intense Li line.

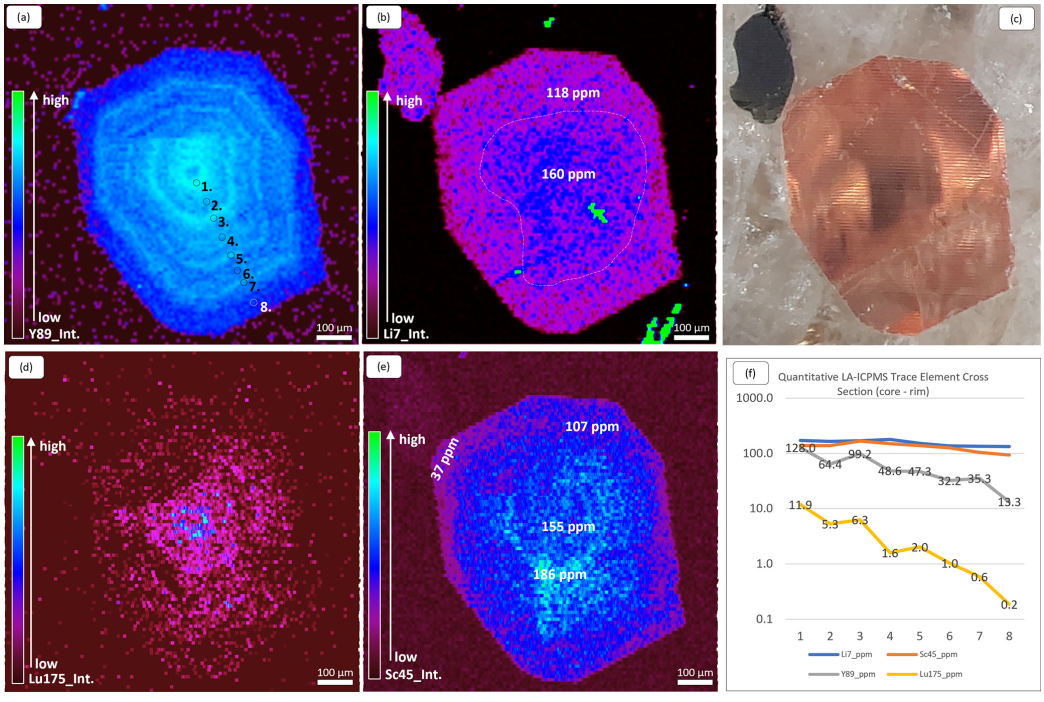

Figure 12. LA-ICP-MS trace element map of one Kietyönmäki garnet grain from the same sample dated using the Lu–Hf method. **(a)** Y intensity map. Note distinct and fine magmatic growth zones. Points indicate locations of RoIs where quantitative concentrations were extracted and are shown on the chart. **(b)** Intensity map of Li. Note the diffuse core of slightly higher Li concentrations. **(c)** Scanned optical image of the mapped garnet grain. **(d)** Lu intensity map mimics the Y intensity, which appears to be a suitable proxy in garnets. **(e)** Sc intensity map correlates vaguely with Li but shows concentric and possible sector zoning. **(f)** Quantitative section construction by eight RoIs, each > 200 pixels, sampling the growth zones.

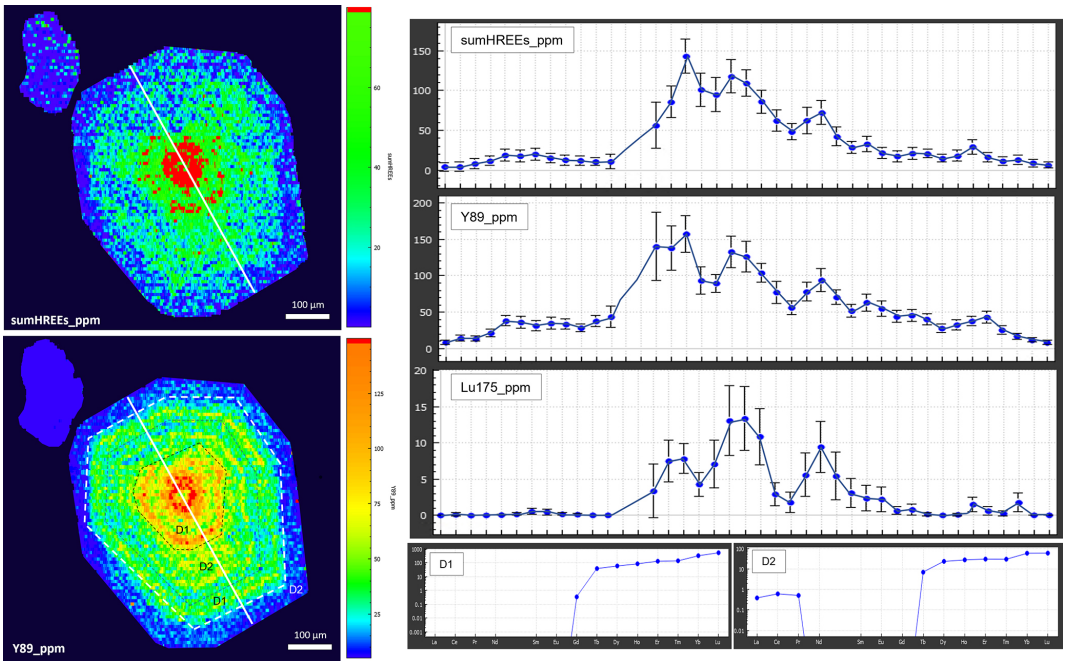

Figure 13. LA-ICP-MS-quantified trace element maps of garnet showing the distribution and concentrations of total heavy rare-earth elements (sumHREEs) and Y. A profile has been made across the grain (white line) showing enrichment of all HREEs and Y in the core. Chondrite-normalised REE plots show two distinct patterns with extreme HREE enrichment in Domain 1 (D1) and with the highest absolute values and LREEs below the detection limit. In Domain 2 (D2) there is a negative MREE anomaly and lower total REE concentrations.

6.3 Lu–Hf garnet geochronology by in situ LA-ICP-MS

Five grains were analysed from a single epoxy mount, producing 54 spot analyses. Two analyses were not included in the age calculation because of the presence of inclusions. The resulting isochron age is 1801 ± 53 Ma (Fig. 10; MSWD = 0.87). Garnet cores have Lu concentrations of 5–10 ppm, and garnet rims have Lu concentrations of 0.4–4 ppm. Spots target both the cores and the rims of the grains; however no age difference was observed between core and rim spots. The enriched Lu composition of the garnet core indicates that the Lu–Hf age obtained from these garnet grains likely represents the crystallisation age.

6.4 Discussion of the Lu–Hf garnet geochronology results

The only other age obtained from pegmatites (Fig. 1) in this region is the U–Pb zircon age by Saalmann et al. (2009), which gave a weighted average $^{207}Pb/^{206}Pb$ age of 1786 ± 7 Ma. Due to the high U content of the zircon grains and their susceptibility to lead loss, Saalmann et al. (2009) suggest that the oldest obtained single grain age of 1815 ± 4 Ma more likely reflects the pegmatite emplacement age. Due to the relatively low Lu contents of the targeted garnet, the Lu–Hf isochron age of this study has significant uncertainty. Consequently, the garnet age is identical within error to the zircon age of Saalmann et al. (2009) and likely reflects the crystallisation age of the pegmatite. For the purposes of this first-pass study, only one pegmatite sample could be targeted.

It is likely that other samples of garnet-bearing pegmatite from Kietyönmäki may have higher Lu contents and produce more precise ages. A future study should target a variety of garnet samples and run micro-X-ray fluorescence (microXRF) maps targeting Y as a proxy for Lu to locate garnet regions with the highest Lu contents. These regions should then be investigated for Lu content using LA-ICP-MS analysis. The samples producing the highest Lu contents are most suitable to be targeted for subsequent Lu–Hf geochronology.

The results of this study are consistent with the zircon age of Saalmann et al. (2009) and suggest that the Kietyönmäki pegmatites are ca. 1790–1815 Ma. This age is consistent with the age of other LCT pegmatites throughout Finland (Lindroos et al., 1996; Alviola et al., 2001) but younger than 1.86 Ga NYF pegmatites occurring in western Finland (Alviola et al., 2001). Further work is required to obtain more precise age constraints and better understand the relationship between the different pegmatite occurrence and NYF and LCT pegmatite families.

7 Conclusions

The Kietyönmäki pegmatite dyke swarm belongs to the rare-element (RE) LCT Li, spodumene–pegmatite type contain-

ing Li, Nb, Ta, and Sn mineralisation. It consists of a main dyke with large 5–25 m width and > 150 m strike lengths with significant Li grades (> 1 Li_2O%) due to the abundance of fine-grained spodumene (SQIs). The SW dyke swarm is composed of narrow 0.3–2 m albite–pegmatite bodies with enrichment of CGMs, garnet, and apatite. Garnet and apatite are almost always present in many LCT pegmatites in Finland as well as worldwide and offer a unique opportunity for novel geochronology applications. In this paper we have obtained the first in situ Lu–Hf garnet date from the Kietyönmäki LCT pegmatite deposit. We demonstrate that the in situ Lu–Hf garnet method can produce reliable dates, in excellent agreement with existing zircon and CGM U–Pb ages. This finding opens up a new opportunity to systematically date pegmatite deposits where zircons are absent or metamict and/or to use this method in parallel with established CGM U–Pb dating to investigate the possible multistage evolution of the pegmatites. We have also presented, for the first time, a detailed LA-ICP-MS quantitative concentration map of a magmatic, pegmatite-hosted garnet from Finland. The results revealed complex textural patterns and concentration levels of Y and HREEs, showing elevated values in the core, and indicated that Y and sumHREEs patterns are the best proxy for elevated Lu (5–12 ppm), which is required for successful Lu–Hf dating. The Lu–Hf garnet method has great potential for understanding the age relationships of LCT pegmatites in Finland.

Data availability. Table S1 containing the Lu–Hf garnet data is available from the EarthChem data repository, https://doi.org/10.60520/IEDA/113207 (Szentpéteri et al., 2024).

Supplement. The supplement related to this article is available online at: https://doi.org/10.5194/ejm-36-433-2024-supplement.

Author contributions. KS: conceptualisation, methodology, investigation, writing (original draft preparation and review and editing). KC: conceptualisation, methodology, investigation, writing (original draft preparation and review and editing). SG: methodology, investigation, writing (review and editing). HOB: methodology, investigation, writing (review and editing). SL: investigation, writing (review and editing). RMM: investigation, writing (review and editing). AB: investigation, writing (review and editing).

Competing interests. The contact author has declared that none of the authors has any competing interests.

Disclaimer. Publisher's note: Copernicus Publications remains neutral with regard to jurisdictional claims made in the text, published maps, institutional affiliations, or any other geographical representation in this paper. While Copernicus Publications makes every effort to include appropriate place names, the final responsibility lies with the authors.

Acknowledgements. The authors would like to acknowledge the chief and associate editors for their careful editorial handling of our manuscript and also Rucheng Wang and the anonymous reviewer, whose comments significantly improved our article.

Financial support. Stijn Glorie's contribution was supported by an Australian Research Council Future Fellowship (grant no. FT210100906).

Review statement. This paper was edited by Rucheng Wang and reviewed by Rucheng Wang and one anonymous referee.

References

Aurola, E.: On the pegmatites in the Torro Area, Southwestern Finland, Bulletin de la Commission Geologique de Finlande, No. 206, 35 pp., https://tupa.gtk.fi/julkaisu/bulletin/bt_206.pdf (last access: 28 May 2024), 1963.

Alviola, R.: The granitic pegmatites of the Somero-Tammela area, in: Symposium Precambrian granitoids. Petrogenesis, geochemistry and metallogeny, 14–17 August 1989, Helsinki, Finland, Excursion C1: Late orogenic and synorogenic Svecofennian granitoids and associated pegmatites of southern Finland. Geol. Surv. Finl, Guidb., 26, 16–25, https://tupa.gtk.fi/julkaisu/opas/op_026.pdf (last access: 28 May 2024), 1989.

Alviola, R.: Tutkimustyöselostus Tammelan kunnassa, valtausalueella Kietyönmäki 1, kaiv. rek, No. 3991/1, suoritetuista teollisuusmineraalitutkimuksista, Geol. Surv. Finl., Rep., no. M06/2024/-93/1/85, 7 pp., 1993 (in Finnish).

Alviola, R.: Pegmatiittien malmipotentiaalista Suomessa, Geol. Surv. Finl, Rep., no.: M10/03/1/85, 5 pp., 2003 (in Finnish).

Alviola, R., Mänttäri, I., Mäkitie, H., and Vaasjoki, M.: Svecofennian rare.element granitic pegmatites of the ostrobothnia region, western finland; their metamorphic environment and time of intrusion, in: Svecofennian granitic pegmatites (1.86–1.79 Ga) and quartz monzonite (1.87 Ga), and their metamorphic environment in the Seinäjoki region, western Finland, edited by: Mäkiite, H., Geol. Surv. Finl. Special Paper, 30, 9–29, 2001.

Anderson, O. M., Lentz, D. R, Mcfalrlae C. R. M., and Falc, H.: A geological, geochemical and textural study of a LCT pegmatite: implications for the magmatic versus metasomatic origin of Nb–Ta mineralization in the Moose II pegmatite, Northwest Territories, Canada, J. Geosci., 58, 299–320, 2013.

Breaks, F. W. and Tindle, A. G.: Rare-Metal Exploration Potential of the Separation Lake Area: an Emerging Target for Bikita-Type Mineralization in the Superior Province of NW Ontario, OGS, OFR 5966, 27 pp., 1997.

Bradley, D. C., McCauley, A. D., and Stillings, L. M.: Mineral-deposit model for lithium-caesium-tantalum pegmatites, USGS Sci. Investig. Rep., 2010-5070-O, 48 pp., 2017.

Černý, P.: Characteristics of pegmatite deposits of tantalum, in: Lanthanides, tantalum and niobium, edited by: Möller, P., Černý, P., Saupé, F., Springer, Berlin Heidelberg New York, 195 pp., https://doi.org/10.1007/978-3-642-87262-4_8, 1989.

Černý, P.: Rare-element granitic pegmatites, Part I: Anatomy and internal evolution of pegmatite deposits, Geoscience Canada (Ore Deposit Models series), 18, 49–67, 1991.

Černý, P.: Geochemical and petrogenetic features of mineralization in rare-element granitic pegmatites in the light of current research, Appl. Geochem., 7, 393–416, 1992.

Černý, P. and Ferguson, R. B.: The Tanco pegmatite at Bernic Lake, Manitoba; IV, Petalite and spodumene relations, Can. Mineral., 11, 660–678, 1972.

Černý, P., Goad, B. E., Hawthorne, F. C., and Chapman, R.: Fractionation trends of the Nb- and Ta- bearing oxide minerals in the Greer Lake pegmatitic granite and its pegmatite aureole, southeastern Manitoba, Am. Mineral., 71, 501–517, 1986.

Černý, P., Novak, M., and Chapman, R.: Effects of sillimanite-grade metamorphism and shearing on Nb-Ta oxide minerals in granitic pegmatites: Marsikov. northern Moravia, Czechoslovakia, Can. Mineral., 30, 699–718, 1992a.

Černý, P., Ercit, T. S., and Wise, M. A.: The tantalite-tapiolite gap: natural assemblages versus experimental data, Can. Mineral., 30, 587–596, 1992b.

Charoy, B., Noronha, F., and Lima, A.: Spodumene–petalite–eucryptite: Mutual relationships and pattern of alteration in Li-rich aplite–pegmatite dykes from northern Portugal, Can. Mineral., 39, 729–746, 2001.

Chischi, J., Oskierski, H. C., Alhadad, M. F., Deditius, A., Senanayake, G., Roberts, M. P., and Dlugogorski, B. Z.: Alteration of Spodumene to Muscovite and Cookeite – Implications for the Fate of Lithium and Iron, Goldschmidt 2021 Abstract, https://conf.goldschmidt.info/goldschmidt/2021/meetingapp.cgi/Paper/4626 (last access: 28 May 2024), 2021.

Dias, F., Lima, A., and Roda-Robles, E.: Mutual relationships between spodumene and petalite from the Iberian Massif pegmatites: More than PT changes?, Can. Mineral., 57, 731–732, 2019.

Eilu, P.: Overview on Gold Deposits in Finland in Mineral Deposits of Finland, edited by: Maier, W. D., O'Brien, H., and Lahtinen, R., Mineral Deposits of Finland, Elsevier, Amsterdam, 377–403, 2015.

Eilu, P., Ahtola, T., Äikäs, O., Halkoaho, T., Heikura, P., Hulkki, H., Iljina, M., Juopperi, H., Karinen, T., Kärkkäinen, N., Konnunaho, J., Kontinen, A., Kontoniemi, O., Korkiakoski, E., Korsakova, M., Kuivasaari, T., Kyläkoski, M., Makkonen, H., Niiranen, T., Nikander, J., Nykänen, V., Perdahl, J.-A., Pohjolainen, E., Räsänen, J., Sorjonen-Ward, P., Tiainen, M., Tontti, M., Torppa, A., and Västi, K.: Metallogenic areas in Finland, Geological Survey of Finland, Special Paper 53, 207–342, https://tupa.gtk.fi/julkaisu/specialpaper/sp_053_pages_207_342.pdf (last access: 28 May 2024), 2012.

Glorie, S., Mulder, J., Hand, M., Fabris, A., Simpson, A., and Gilbert, S.: Laser ablation (in situ) Lu-Hf dating of magmatic fluorite and hydrothermal fluorite-bearing veins, Geosci. Front., 14, 101629, https://doi.org/10.1016/j.gsf.2023.101629, 2023.

Kuusela, J., Ahtola, T., Koistinen, E., Seppänen, H., Hatakka, T., and Lohva, J.: Report of investigations on the Rapasaaret lithium pegmatite deposit in Kaustinen-Kokkola, Western Finland, Geol. Surv. Finl., Rep., 42/2011, 65 pp., https://tupa.gtk.fi/raportti/arkisto/42_2011.pdf (last access: 28 May 2024), 2011.

Leväniemi, H.: Lithium Pegmatite Prospectivity Modelling in Somero-Tammela Area, Southern Finland, Geol. Surv. Finl., Rep., 151/2013, 20 pp., https://tupa.gtk.fi/raportti/arkisto/151_2013.pdf (last access: 28 May 2024), 2013.

Li, Y. and Vermeesch, P.: Short communication: Inverse isochron regression for Re–Os, K–Ca and other chronometers, Geochronology, 3, 415–420, https://doi.org/10.5194/gchron-3-415-2021, 2021.

Lima, A. and Dias, F.: Spodumene and Quartz Intergrowth – Textural and Genesis Point of View, Geophys. Res. Abstr., EGU General Assembly 2019, Vienna, Austria, Vol. 21, EGU2019-13404, https://meetingorganizer.copernicus.org/EGU2019/EGU2019-13404.pdf (last access: 28 May 2024), 2019.

Lindroos, A., Romer, R. L., Ehlers, C., and Alviola, R.: Late-orogenic Svecofennian deformation in SW Finland constrained by pegmatite emplacement ages, Terra Nova, 8, 567–574, https://doi.org/10.1111/j.1365-3121.1996.tb00786.x, 1996.

London, D.: Experimental phase equilibria in the system $LiAlSiO_4$–SiO_2-H_2O: a petrogenetic grid for lithium-rich pegmatites, Am. Mineral., 69, 995–1004, 1984.

London, D.: Pegmatites, Can. Mineral. Spec. Publ., Québec, QC, Canada, 10, 340 pp., ISBN 9780921294474, 2008.

Lyalina, L. M., Selivanova, E. A., and Hatert, F.: Nomenclature of the triphylite group of minerals, Eur. J. Mineral., 35, 427–437, https://doi.org/10.5194/ejm-35-427-2023, 2023.

Hernández-Filiberto, L., Roda-Robles, E., Simmons, W. B., and Webber, K. L.: Garnet as Indicator of Pegmatite Evolution: The Case Study of Pegmatites from the Oxford Pegmatite Field (Maine, USA), Minerals, 11, 802–810, https://doi.org/10.3390/min11080802, 2021.

Mäkinen, E.: Die Granitpegmatite von Tammela in Finnland und ihire Minerale, Bulletin de la Commission Geologique de Finlande No. 35 (BGSF), 101 pp., https://tupa.gtk.fi/julkaisu/bulletin/bt_035.pdf (last access: 28 May 2024), 1913.

Martins, T. C.: Multidisciplinary study of pegmatites and associated Li and Sn-Nb-Ta mineralisation from the Barroso-Alvão region, PhD Thesis, Faculty of Sciences, University of Porto, 269 pp., https://repositorio-aberto.up.pt/handle/10216/83857 (last access: 28 May 2024), 2009.

Moretz, L., Heimann, A., Bitner, J., Wise, M., Rodrigues Soares, D., and Mousinho, F. A.: The composition of garnet as indicator of rare metal (Li) mineralization in granitic pegmatites, Proceeding of the 6th International Symposium on Granitic Pegmatites, New Hampshire and Maine, USA, 26 May–2 June, 94–95, 2013.

Müller, A., Kaersley, A., Spratt, J., and Seltmann, R.: Petrogenetic implications of magmatic garnet in granitic pegmatites from southern Norway, Can. Mineral., 50, 1095–1115, 2012.

Nebel, O., Morel, M. L. A., and Vroon, P. Z.: Isotope dilution determinations of Lu, Hf, Zr, Ta and W, and Hf isotope compositions of NIST SRM 610 and 612 glass wafers, Geostand. Geoanal. Res., 33, 487–499, https://doi.org/10.1111/j.1751-908X.2009.00032.x, 2009.

Norris, A. and Danyushevsky, L.: Towards estimating the complete uncertainty budget of quantified results measured by LA-ICP-MS, Goldschimdt Boston, https://goldschmidtabstracts.info/2018/1894.pdf (last access: 28 May 2024), 2018.

Pan, Y. and Breaks, F. W.: Rare earth elements in fluorapatite, separation lake area, Ontario: evidence for S-type granite – rare element pegmatite linkage, Can. Mineral., 35, 659–671, 1997.

Paton, C., Hellstrom, J., Paul, B., Woodhead, J., and Hergt, J.: Iolite: Freeware for the visualisation and processing of mass spectrometric data, J. Anal. Atom. Spectrom., 26, 2508–2518, https://doi.org/10.1039/c1ja10172b, 2011.

Paul, B., Paton, C., Norris, A., Woodhead, J., Hellstrom, J., Hergt, J., and Greig, A.: CellSpace: A module for creating spatially registered laser ablation images within the Iolite freeware environment, J. Anal. Atom. Spectrom., 27, 700–706, https://doi.org/10.1039/c2ja10383d, 2012.

Petrus, J. A., Chew, D. M., Leybourne, M. I., and Kamber, B. S.: A new approach to laser-ablation inductively-coupled-plasma mass-spectrometry (LA-ICP-MS) using the flexible map interrogation tool "Monocle", Chem. Geol., 463, 76–93, 2017.

Pouchou, J. L. and Pichoir, F.: Quantitative Analysis of Homogeneous or Stratified Microvolumes Applying the Model "PAP", in: Electron Probe Quantification, edited by: Heinrich, K. F. J. and Newbury, D. E., Plenum Press, New York, 31–75, 1991.

Romer, R. L. and Smeds, S.-A.: U-Pb columbite ages of pegmatites from Sveconorwegian terranes in southwestern Sweden, Precambrian Res., 76, 15–30, https://doi.org/10.1016/0301-9268(95)00023-2, 1996.

Roza Llera, A., Fuertes-Fuente, M., Cepedal, A., and Martin-Izard, A.: Barren and Li–Sn–Ta Mineralized Pegmatites from NW Spain (Central Galicia): A Comparative Study of Their Mineralogy, Geochemistry, and Wallrock Metasomatism, Minerals, 9, 739, https://doi.org/10.3390/min9120739, 2019.

Saalmann, K.: Structural control on gold mineralization in the Satulinmäki and Riukka prospects, Häme Schist Belt, southern Finland, B. Geol. Soc. Finland, 79, 69–93, 2007.

Saalmann, K., Mänttäri, I., Ruffet, G., and Whitehouse, M. J.: Age and tectonic framework of structurally controlled Palaeoproterozoic gold mineralization in the Häme belt of southern Finland, Precambrian Res., 174, 53–77, 2009.

Saikkonen, R.: Hirvikallion petaliittiesiintymä, Tammela, Oy Lohja Ab, Malminetsintä, Report 12.1.1981, 1981 (in Finnish).

Simonen, A.: Kalioperäkartan selitys, Lehti – Sheet – 2024, Somero, Explanation to the map of rocks, Geological map of Finland, 1 : 100 000, https://tupa.gtk.fi/kartta/kallioperakartta100/kps_2024.pdf (last access: 28 May 2024), 1956.

Simpson, A., Gilbert, S., Tamblyn, R., Hand, M., Spandler, C., Gillespie, J., Nixon, A., and Glorie, S.: In-situ Lu-Hf geochronology of garnet, apatite and xenotime by LA-ICP MS/MS, Chem. Geol., 577, 120299, https://doi.org/10.1016/j.chemgeo.2021.120299, 2021.

Simpson, A., Glorie, S., Hand, M., Spandler, C., Gilbert, S., and Cave, B.: In situ Lu-Hf geochronology of calcite, Geochronology, 4, 353–372, https://doi.org/10.5194/gchron-4-353-2022, 2022.

Simpson, A., Glorie, S., Hand, M., Spandler, C., and Gilbert, S.: Garnet Lu-Hf speed dating: A novel method to rapidly resolve polymetamorphic histories, Geosci. Front., 121, 215–234, https://doi.org/10.1016/j.gr.2023.04.011, 2023.

Söderlund, U., Patchett, P. J., Vervoort, J. D., and Isachsen, C. E.: The 176Lu decay constant determined by Lu-Hf and U-Pb isotope systematics of Precambrian mafic intrusions, Earth Planet. Sc. Lett., 219, 311–324, https://doi.org/10.1016/S0012-821X(04)00012-3, 2004.

Szentpéteri, K., Cutts, K., Glorie, S., O'Brien, H., Lukkari, S., Michallik, R. M., and Butcher, A.: Laser ablation ICP-MS/MS Lu-Hf garnet data for Keityonmaki Li-pegmatite, Version 1.0., Interdisciplinary Earth Data Alliance (IEDA) [data set], https://doi.org/10.60520/IEDA/113207, 2024.

Teertstra, D. K., Černý, P., and Hawthorne, F. C.: Rubidium-rich feldspars and associated minerals from the Luolämaki pegmatite, Somero, Finland, BGSF, 70, 43–49, 1998.

Teertstra, D. K., Černý, P., and Hawthorne, F. C.: Pollucite and its alteration in Finnish pegmatites, BGSF, 368, 39 pp., https://tupa.gtk.fi/julkaisu/bulletin/bt_368.pdf (last access: 28 May 2024), 1993.

Thomas, R. J., Bühmann, D., Bullen, W. D., Scogings, A. J., and De Bruin, D.: Unusual spodumene pegmatites from the Late Kibaran of southern Natal, South Africa, Ore Geol. Rev., 9, 61–182, 1994.

Tindle, A. G. and Breaks, F. W.: Columbite-tantalite mineral chemistry from rare-element granitic pegmatites: Separation Lake area, N.W. Ontario, Canada, Mineral. Petr., 70, 165–198, 2000.

Vermeesch, P: IsoplotR: a free and open toolbox for geochronology, Geosci. Front., 9, 1479–1493, https://doi.org/10.1016/j.gsf.2018.04.001, 2018.

Vesasalo, A.: On the petalite occurrences of Tammela, SW Finland, BGSF, 31, 59–74, 1959.